Journal of Molecular Structure 1234 (2021) 130192

Contents lists available at ScienceDirect

Journal of Molecular Structure

journal homepage: www.elsevier.com/locate/molstr

Synthesis, characterization, DFT calculations, protein binding and molecular docking studies of mononuclear dioxomolybdenum(VI) complexes with ONS donor ligand

Malini Roy[a], Debanjana Biswal[a], Oiendrilla Sarkar[a], Nikhil Ranjan Pramanik[b,*], Suvendu Paul[c], Chandan Kumar Manna[d], Tapan Kumar Mondal[d], Syamal Chakrabarti[a,*]

[a] Department of Chemistry, University College of Science, 92, Acharya Prafulla Chandra Road, Kolkata,700009, West Bengal, India
[b] Department of Chemistry, Bidhannagar College, EB-2, Sector-1, Salt Lake, Kolkata 700064, India
[c] Department of Chemistry, University of Kalyani, Kalyani, Nadia, West Bengal, 741235, India
[d] Department of Chemistry (Inorganic Section), Jadavpur University, Kolkata 700032, India

ARTICLE INFO

Article history:
Received 6 January 2021
Revised 20 February 2021
Accepted 22 February 2021
Available online 25 February 2021

Keywords:
Dioxomolybdenum(VI)
ONS donor ligand
DFT calculations
Protein interaction
Molecular docking

ABSTRACT

Several new dioxomolybdenum(VI) complexes containing tridentate ONS donor ligand (H_2L) derived from pyridoxal and S-benzyldithiocarbazate have been synthesized by refluxing $MoO_2(acac)_2$ with Schiff base ligand and Lewis base (B) (where, B = pyridine, γ-picoline, 1-methylimidazole, tetrahydrofuran) in 1:1:1.5 molar proportions in methanol. The complexes having general formula MoO_2LB (**1**–**4**) are thoroughly characterized by elemental analyses and various spectroscopic techniques (IR, ^1H NMR, UV–Vis and mass spectra). The structures of the complexes have been optimized by Density Functional Theory (DFT) calculations. The hexa coordinated metal center possesses a distorted octahedral geometry in all the complexes. The redox behavior of the complexes is studied by cyclic voltammetry. The oxo-transfer reactivity of the MoO_2LB complexes with PPh_3 has also been examined. The interactions of the complexes with Bovine Serum Albumin (BSA) protein are investigated spectroscopically by absorption, fluorescence titration and fluorescence life time measurements. The values of the Stern-Volmer constant (K_{SV}), binding constant (K_b) and number of binding sites (n) are determined which indicates significant binding with BSA protein. Fluorescence spectral change also indicates efficient FRET from the protein to ligand and complexes. Molecular docking studies have also been carried out to understand the binding modes and interaction patterns of the dioxomolybdenum(VI) complexes with BSA.

1. Introduction

The chemistry of molybdenum has been widely explored due to its versatility in several fields. It constitutes the active site of so many metalloenzymes such as hydroxylase [1], oxotransferases [2] and nitrogenase [3]. The biochemical role of molybdenum is based on its ability to facilitate electron exchange and coordinate with a variety of ligands containing different donor environments [4]. The useful role of molybdenum is not restricted to biological systems alone, but it also exhibits catalytic activities in a variety of chemical reactions like epoxidation of olefins [5], olefin metathesis [6] and ammoxidation of propenes [7]. Oxygen atom transfer (OAT), in both nature and industry also involves the reduction of mononuclear Mo(VI) moiety by PPh_3 towards Mo(IV) complexes [8].

Pyridoxal [3–hydroxy-5-(hydroxymethyl)-2-methyl pyridine-4-carbaldehyde] is one of three natural forms of Vitamin B6 and is present as cofactor in various enzymatic processes [9]. Pyridoxal and its derivatives also exhibit significant roles in treatment and the prevention of cancer [10]. The presence of pyridoxal as one of the building block of the ligand is quite advantageous as it is not expected to give rise any toxic metabolites and improve the solubility of the final complexes.

Dithiocarbazates and their metal complexes are very much interesting scaffolds and possess anticancer, antibacterial, antifungal and insecticidal activities [11]. The Schiff base ligands derived from pyridoxal draw a remarkable attention by displaying a variety of coordination sites with both hard/soft character [12]. The aldehyde group attached to the pyridine moiety can enable the tuning of the properties of the metal complexes [13] by protonation deprotonation of the pyridine N.

* Corresponding authors.
E-mail addresses: nr_pramanik@yahoo.co.in (N.R. Pramanik), schakrabarti2014@gmail.com (S. Chakrabarti).

https://doi.org/10.1016/j.molstruc.2021.130192
0022-2860/

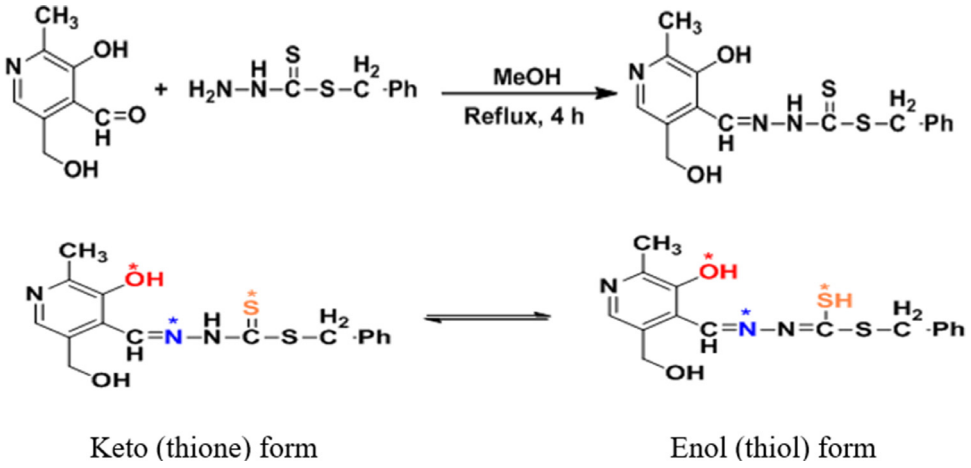

Scheme 1. Reaction diagram for the preparation of the ligand.

Biological applicability of the complexes can be understood by examining their interactions with serum albumin (SA) proteins. Among the serum albumins bovine serum albumin (BSA) has wide applications due to its low cost, high availability and structural homology with human serum albumins (HSA) [14].

Knowing the fact up till now, a few molybdenum complexes containing pyridoxal based Schiff based ligands [15–17] have been reported earlier. Their syntheses, structural, stereochemical, spectroscopic and electrochemical properties are quite fascinating.

In this paper, we report the synthesis and characterization of four mononuclear dioxomolybdenum(VI) complexes of general formula MoO_2LB [B = Pyridine (**1**), γ-picoline (**2**), 1-methyl imidazole (**3**), tetrahydrofuran (**4**)] having pyridoxal-S-benzyldithiocarbazate as the ligand (H_2L). The complexes have been characterized by elemental analyses, various spectroscopic (IR, UV–Vis, ^{1}H NMR and mass spectra) techniques and cyclic voltammetry. The optimized structures and the electronic properties of the complexes have been elucidated by DFT calculations. To investigate the bio applicability the interaction of the compounds with BSA protein has also been performed utilizing absorption, fluorescence titration and time resolved fluorescence measurements. All the synthesized compounds show strong fluorescence resonance energy transfer (FRET) from BSA to the ligand and Mo(VI) complexes. Molecular docking studies were carried out to understand the binding interactions of the synthesized compounds with BSA protein.

2. Materials and methods

2.1. Materials

Pyridoxal.HCl was purchased from HIMEDIA. The precursors, S-benzyldithiocarbazate [18], $MoO_2(acac)_2$ were prepared as described in literature [19]. THF, 1-methylimidazole, pyridine and γ-picoline are of reagent grade, commercially available and used without further purification. The solvents used here were reagent grades. Methanol and ethanol were dried using Mg turnings & iodine and then distilled.

2.2. Synthesis of the ligand (H_2L)

Pyridoxal.HCl was neutralized using an equivalent amount of KOH following the literature method [20]. The Schiff base ligand was then prepared by refluxing of neutral pyridoxalhydrochloride (1.02 g, 5.0 mmoL) and S-benzyl dithiocarbazate (0.99 g, 5.0 mmoL) in Ca. 40 ml MeOH on a water bath for 4 h (Scheme 1) [21]. Yellow amorphous solid was obtained as ligand which was satisfactorily characterized by elemental analyses, IR, ^{1}H NMR and mass spectra.

Yield: 88%, M.P. > 200^{0}C, Anal. Calcd. for $C_{16}H_{17}N_3O_2S_2$ (%): C, 55.33; H, 4.89; N, 12.10. Found: C, 55.25; H, 4.75; N, 11.93. Selected IR (KBr Pellet), cm^{-1}: $\nu_{(O-H)}$ 3273 (m), $\nu_{(N-H)}$ 3078 (m), $\nu_{(C=N)}$ 1640 (s), $\nu_{(C=S)}$ 1309 (s);^{1}H NMR (DMSO–d_6, δ/ppm): (-CH=*N*) 8.01 s (1H), (-S-CH_2-Ph) 4.49 s (2H), (Aromatic protons) 7.24–7.36 m (6H), (-CH_3) 2.43 s (3H), (-CH_2OH) 4.69 s (OH). ESI-MS (+) in MeOH: *m/z* 348 (*M* + *H*).

2.3. Synthesis of the complexes

[MoO_2L(py)] (**1**). A mixture of $MoO_2(acac)_2$ (0.33 g, 1.0 mmoL) and H_2L (0.35 g, 1.0 mmoL) in dry MeOH was refluxed for 2 h. To this solution, 2–3 drops of pyridine was added. The resulting yellowish orange solution then refluxed for another 2 h. The solution was filtered. After one day, upon cooling yellowish amorphous compound was obtained from the filtrate. Yield ~72%. Anal. Calcd. for $C_{21}H_{20}N_4O_4S_2Mo$ (%): C, 45.65; H, 3.62; N, 10.15; Mo, 17.39. Found: C, 45.48; H, 3.50; N, 10.10; Mo, 16.92. Selected IR (KBr Pellet), cm^{-1}: $\nu_{(O-H)}$ 3385 (m), $\nu_{(C\ =\ N)}$ 1593 (m), $\nu_{(Mo=O)}$ 895 (vs), 931 (s), $\nu_{(Mo-N)}$ 694 (m), $\nu_{(Mo-S)}$ 492 (m). UV–Vis (MeOH) [λ_{max}/nm (ε/dm^3 mol^{-1}cm^{-1})]: 234 (9900), 332 (10,000), 368 sh (6400), 420 sh (2010). ^{1}H NMR (DMSO–d_6, δ/ppm): (-CH=*N*) 9.09 s (1H), (-S-CH_2-Ph) 4.38 s (2H), (Aromatic protons) 7.02–7.98 m (11H), (-CH_3) 2.43 s (3H), (-CH_2OH) 4.66 s (OH). ESI-MS (+) in MeOH: *m/z* 552 (M).

The complexes [MoO_2L(γ-pic)] (**2**) and [MoO_2L(1-methyl imz)] (**3**), were prepared similarly by refluxing with the appropriate monodentate Lewis bases like γ-picoline and 1-methyl imidazole in dry MeOH.

[MoO_2L(γ-pic)] (**2**). Yield ~81%. Anal. Calcd. for $C_{22}H_{22}N_4O_4S_2Mo$ (%): C, 46.64; H, 3.89; N, 9.89; Mo, 16.96. Found: C, 46.32; H, 3.68; N, 9.75; Mo, 17.10. Selected IR (KBr Pellet), cm^{-1}: $\nu_{(O-H)}$ 3410 (m), $\nu_{(C\ =\ N)}$ 1595 (m), $\nu_{(Mo=O)}$ 901 (s), 934 (s), $\nu_{(Mo-N)}$ 695 (m), $\nu_{(Mo-S)}$ 475 (m); UV–Vis (MeOH) [λ_{max}/nm (ε/dm^{3}mol^{-1}cm^{-1})]: 231 (7400), 337 (11,300), 365 (8900), 421 sh (1170).^{1}H NMR (DMSO–d_6, δ/ppm): (Py-CH_3) 2.37 s (3H), (-CH=*N*) 9.12 s (1H), (-S-CH_2-Ph) 4.46 s (2H), (Aromatic protons) 7.29–7.47 m (10H), (-CH_3) 2.50 s (3H), (-CH_2OH) 4.74 s (OH). ESI-MS (+) in MeOH: *m/z* 590 (*M* + *H*+Na).

[MoO_2L(1-methyl imz)] (**3**). Yields~78%. Anal. Calcd. for $C_{20}H_{21}N_5O_4S_2Mo$ (%): C, 43.24; H, 3.78; N, 12.61; Mo, 17.29. Found: C, 43.18; H, 3.68; N, 12.58; Mo, 17.12. Selected IR (KBr Pellet), cm^{-1}: $\nu_{(O-H)}$ 3385 (m), $\nu_{(C\ =\ N)}$ 1585 (m), $\nu_{(Mo=O)}$ 915 (vs), 939 (s), $\nu_{(Mo-N)}$ 694 (m), $\nu_{(Mo-S)}$ 476 (m); UV–Vis (MeOH) [λ_{max}/nm

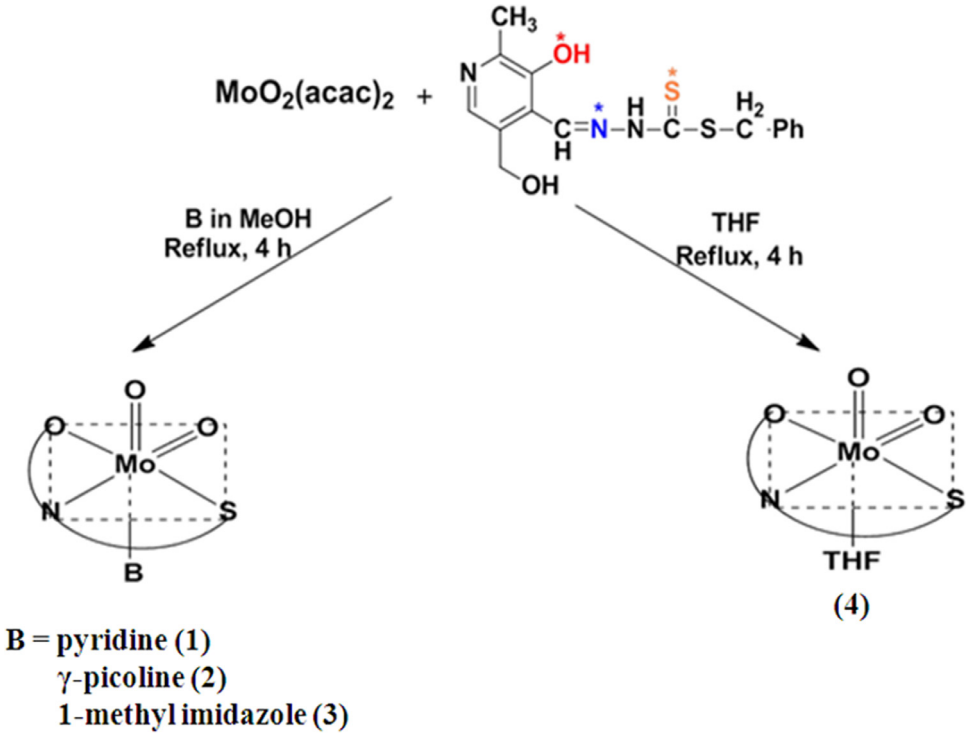

Scheme 2. Reaction diagram for the preparation of the complexes.

(ε/dm^3 mol^{-1}cm^{-1})]: 212 (11,000), 330 (3200), 433 (700). ^{1}H NMR (DMSO–d_6, δ/ppm): (imz-N-CH_3) 3.67 s (3H), (-CH=*N*) 8.70 s (1H), (-S-CH_2-Ph) 4.37 s (2H), (Aromatic protons) 7.23–7.35 m (9H), (-CH_3) 2.41 s (3H), (-CH_3OH) 4.53 s (OH). ESI-MS (+) in MeOH: *m/z* 555 (M).

[MoO_2L(THF)] (4). The complex was prepared by refluxing a solution of MoO_2(acac)$_2$ (0.33 g, 1.0 mmoL) and H_2L (0.35 g, 1.0 mmoL) in 20 ml dry THF for 4 h (Scheme 2). The solution was filtered and filtrate was kept at room temperature. After one day greenish yellow amorphous compound was obtained from the filtrate. Yield: ~76%. Anal. Calcd. for $C_{20}H_{23}N_3O_5S_2Mo$ (%): C, 44.04; H, 4.22; N, 7.71; Mo, 17.61. Found: C, 43.97; H, 4.10; N, 7.62; Mo, 16.85. Selected IR (KBr Pellet), cm^{-1}: $\nu_{(O-H)}$ 3372 (m), $\nu_{(C\ =\ N)}$ 1580 (m), $\nu_{(Mo=O)}$ 907 (vs), 943 (s), $\nu_{(Mo-N)}$ 696 (m), $\nu_{(Mo-S)}$ 460 (m); UV–Vis (MeOH) [λ_{max}/nm (ε/dm^3 mol^{-1}cm^{-1})]: 216 (13,000), 271 (11,000), 324 (5400), 431 (1200).^{1}H NMR (DMSO–d_6, δ/ppm): (THF protons) 1.93–2.08 m (4H) and 3.42–3.59 m (4H), (-CH=*N*) 9.09 s (1H), (-S-CH_2-Ph) 4.38 s (2H), (Aromatic protons) 7.18–7.38 m (6H), (-CH_3) 2.41 s (3H), (-CH_2OH) 4.66 s (OH). ESI-MS (+) in MeOH: *m/z* 545 (M).

Reaction diagrams for the preparation of all the complexes are shown in Scheme 2.

Despite many attempts no suitable crystals of the synthesized complexes could be obtained for X-ray diffraction.

2.4. Physical measurements

Elemental analyses were performed on a Perkin-Elmer 240 C, H, N analyzer. NMR spectra were recorded on a Bruker 300 L NMR spectrometer operating at 300 MHz with TMS as internal standard. IR spectra were recorded as KBr pellets on a Perkin-Elmer model 883 infrared spectrophotometer. Electronic spectra were recorded using a HITACHI U-3501 UV–Vis recording spectrophotometer. Magnetic susceptibility was measured with a PAR model 155 vibrating sample magnetometer with Hg [Co(SCN)$_4$] as calibrant. Electrochemical data were collected on a Sycopel model AEW2 1820 F/S instrument at 298 K using a Pt working electrode, Pt auxiliary electrode and SCE reference electrode. Cyclic voltammograms were recorded in DMF containing 0.1 M TBAP as supporting electrolyte. Mass spectra were recorded by a Waters XIVO GTS QTOF spectrometer.

2.5. Computational methods

Gas phase geometry of the complexes were fully optimized without any symmetry constraints in singlet ground-state by DFT/B3LYP [22,23] method. The hybrid B3LYP is widely used for molybdenum complexes [8, 24–26]. All elements except molybdenum were assigned the 6–31+*G*(d) basis set. For Mo atom SDD basis set with effective core potential was employed [27,28]. Vibrational frequency calculation was performed on the optimized geometries to ensure that there is no imaginary frequency. Electronic spectrum was computed using the time-dependent density functional theory (TDDFT) formalism [29–31] and the solvent effect (methanol) was simulated using the conductor-like polarizable continuum model (CPCM) [32–34]. All computations were carried out using the Gaussian09 (G09) program [35]. GaussSum [36] program was used to calculate the fractional contributions of various groups to each molecular orbital for the complexes.

2.6. Protein interaction study

2.6.1. Absorption study of the compounds with BSA protein

Bovine serum albumin (BSA) was purchased from Sigma-Aldrich. A stock solution of BSA (10^{-5} M) was prepared by dissolving measured amount of BSA in phosphate buffer (pH = 7) and preserved at 4 °C for further use. Stock solutions of the compounds were prepared in 10^{-4} M concentration in dry ethanol. Absorption spectra were recorded using a Hitachi U-3501 UV–Vis spectrophotometer. BSA (2 mL, 10^{-5} M) was titrated with successive addition of the compounds (0–20 µL) using a micropipette.

2.6.2. Fluorescence quenching study of the compounds with BSA protein

To investigate the interaction between BSA and the synthesized compounds, emission spectra were recorded on a PerkinElmer LS55 fluorescence spectrometer with rectangular quartz cuvette of 1 cm path length at a fixed excitation wavelength corresponding to BSA at 278 nm and monitoring the emission at 356 nm at room temperature. The excitation and emission slit widths and scan rates were constantly maintained for all the experiments. 2 mL BSA solution (10^{-5} M) was titrated by successive addition of 10^{-4} M compound solution (0–20 µL).

2.6.3. Fluorescence life time measurement

Fluorescence lifetimes were measured by the method of Time Correlated Single-Photon Counting (TCSPC) using a HORIBA Jobin Yvon Fluorocube-01-NL fluorescence lifetime spectrometer. 2 ml BSA solution (10^{-5} M) was titrated by incremental addition of 10^{-4} M compound solutions (0–20 µL). The sample was excited using a laser diode at 291 nm. The decays were analyzed using DAS-6 decay analysis software. The fluorescence decay curves were analyzed by biexponential fitting program of IBH.

2.6.4. Molecular docking studies

There must be some meaningful interactions between the ligands and BSA, behind the spectroscopic changes observed in the previous section. To insight the interactions at molecular level, docking analysis of BSA was performed with H_2L and its Mo complexes. The docking was performed using Auto Dock (4.2) software package [37]. Analysis and presentation of the docked structures were performed with PyMOL 1.3 program package [38]. At first, H_2L and its Mo complexes were optimized in vacuum employing DFT/B3LYP [22,23] theoretical model. All elements except molybdenum were assigned the 6–31+*G*(d) basis set. For Mo atom SDD basis set with effective core potential was employed [27, 28, 39] in Gaussian 09 W software package [35]. On the other hand, crystal structure of BSA (PDB ID: 3V03) from RCSB Protein Data Bank [40] was considered for docking. Initially, the water molecules and other irrelevant information of the crystal structure were eliminated. Then, between the two equivalent chains (A and B) of BSA, chain B was removed using Auto Dock 4.2 and rest part was considered as receptor for docking. Since among all the amino acid components of BSA, only tryptophan is responsible for intrinsic fluorescence of BSA, two tryptophan units (TRP 134 & TRP 213) were considered as flexible and rest as fixed residue. The grid box was chosen to be significantly large to include not only the receptor portion but also covering the ligand too. Therefore, 126 × 126 × 126 Å grid points and 0.753 Å grid spacing with grid center at 38.223, 22.622, 40.920 were developed through AutoGrid. The Lamarckian genetic algorithm (LGA) was employed for docking calculations. Default values were taken for other docking parameters. For better presentation of docked comlplexes PyMOL 1.3 [38] was employed.

3. Results and discussion

3.1. Synthesis

The Schiff base ligand H_2L was prepared by condensing S-benzyl dithiocarbazate with pyridoxal hydrochloride in dry methanol by the method reported previously [21]. The ligand was satisfactorily characterized by elemental analyses, IR, ^{1}HNMR and mass spectra.

The complexes having general formula MoO_2LB [where, *B* = pyridine (**1**), γ-picoline (**2**), 1-methyl imidazole (**3**)], have been synthesized by refluxing the equimolar amount of $MoO_2(acac)_2$ and the ligand in presence of slight excess of corresponding Lewis base. Complex **4** has been synthesized by refluxing equimolar proportions of $MoO_2(acac)_2$ and the ligand (H_2L) in dry THF medium.

Yellowish colored MoO_2LB complexes are air stable in the solid state. They are rarely soluble in nonpolar solvents but readily soluble in polar solvents like MeOH, DMSO, DMF etc. The complexes are diamagnetic due to presence of d^0 Mo(VI) center [41]. All the complexes are satisfactorily characterized by elemental analyses, various spectroscopy (IR, UV–Vis, ^{1}H NMR and mass spectrometry) and electrochemically. Relevant DFT calculations have been carried out to propose the molecular geometry of the complexes. To check the biological importance of the investigated complexes, protein binding study and molecular docking have also been performed with BSA.

3.2. IR spectra

Characteristic IR bands of the dioxomolybdenum(VI) complexes are given in the experimental section and the spectra are shown in Fig. S1. A strong band around 1640 cm^{-1} is observed for the ligand H_2L due to presence of $\nu_{(C=N)}$ which is red shifted and found in the region 1580–1595 cm^{-1} for the complexes [42]. The $\nu_{(C=S)}$ band observed in 1309 cm^{-1} for the ligand disappeared upon complex formation [8] The complexes possess a medium intensity band around 694–696 cm^{-1} region for $\nu_{(Mo\text{-}N)}$ stretching vibrations. Another band is found in the region 460–492 cm^{-1} for $\nu_{(Mo\text{-}S)}$ stretching vibrations. Two intense IR bands are observed in 895–943 cm^{-1} region which can be assigned as $Mo{=}O_t$ symmetric and anti symmetric stretching modes of *cis*-$[MoO_2]^{2+}$ moiety [43]. Both the ligand and the complexes possess a broad band in 3273–3410 cm^{-1} due to -CH_2-OH stretching mode indicating that the alcoholic -OH is not involved in complexation.

The strong bands in the range 1453–1490 cm^{-1} characteristic of $\nu_{(Mo\text{-}N)}/\nu_{(Mo\text{-}O)}$ stretching vibrations confirm the presence of the coordinated Lewis bases like pyridine, γ-picoline, 1-methyl imidazole and tetrahydrofuran. Two strong bands at 1490 and 1286 cm^{-1} and a sharp band of medium intensity at 1046 cm^{-1} confirms the presence of γ-picoline in complex **2** [44]. On the other hand, complex **3** and **4** possess two medium intensity bands at 1071 and 1140 cm^{-1} which correspond to $\nu_{(N\text{–}C)}$ of 1-methyl imidazole and $\nu_{(C\text{–}O)}$ of tetrahydrofuran respectively.

3.3. Electronic spectra

Electronic spectra of the dioxomolybdenum(VI) complexes were recorded in dry methanol and the spectral data are given in the experimental section and the spectra of all the complexes are presented in Fig. S2. The complexes **1**–**4** show characteristic band in the range of 420–433 nm due to S($p\pi$)→Mo($d\pi$) LMCT transition [44] by promoting of an electron from filled HOMO of the ligand, primarily S($p\pi$) in character, to the empty LUMO of the Mo($d\pi$) character. Another LMCT bands observed in the range of 271–368 nm may be assigned as nitrogen to molybdenum and oxygen to molybdenum charge transfer transitions [45]. Other high energy transitions arising in the range of 212–234 nm may be due to intraligand transitions.

3.4. ^{1}H NMR spectra

^{1}H NMR spectra of the ligand and the complexes were recorded in DMSO–d_6 solvent and the spectral data are summarized in the experimental section. The free ligand exhibits two characteristic signals at δ 11.20 and 10.08 ppm due to O–H and N–H which are found to disappear in the complexes. The singlet signal at δ 8.01 ppm arises due to azomethine proton (-CH=*N*) in the ligand

Table 1

Complexes	E_{pc} (V)		E_{pa} (V)
	Mo^{VI}/Mo^{V}	Mo^{V}/Mo^{IV}	Mo^{IV}/Mo^{VI}
MoO_2L(py) (1)	− 0.59	− 1.32	+ 0.95
MoO_2L(γ-pic) (2)	− 0.43	− 1.28	+ 0.94
MoO_2L(1-methyl imz) (3)	− 0.62	− 1.25	+ 0.99
MoO_2L(THF) (4)	− 0.60	− 1.06	+ 0.90

[a]*Solvent:* DMF (dry, degassed); supporting electrolyte: 0.1 M TBAP; solution strength: 10^{-3} M; working electrode: platinum; reference electrode: SCE; scan rate: 100 mVs^{-1}.

which is shifted to δ 9.09, 9.12, 8.70 and 9.09 ppm in the corresponding complexes **1, 2, 3** and **4** respectively indicating the involvement of azomethine nitrogen in complexation. The methylene protons in the ligand and the complexes appear at δ 4.49, 4.38, 4.46, 4.37 and 4.38 ppm which imply that S-benzyl sulfur is not involved in coordination. The aromatic protons give characteristic multiplets in the range δ 7.02–7.98 ppm in both the ligand and the complexes. The $-CH_3$ and aliphatic –OH group of pyridoxal moiety resonate at δ 2.41–2.50 ppm and δ 4.53–4.74 ppm respectively in the ligand and the complexes. In complex **2** and **3**, the $-CH_3$ group in the substituted pyridine and imidazole ring show their usual proton signals. Similarly in complexes **1** and **4** the ring protons of pyridine and THF exhibit their usual chemical shifts.

3.5. Mass spectrometry

The molecular formulation and the structural information can be obtained from the ESI-MS analysis. The mass spectra of the ligand and the complexes are recorded in MeOH and the spectral data are given in experimental section. The mass spectra of the ligand and the complexes show molecular ion peaks at *m/z* 348 ($M + H$), 552 (M), 590 ($M + H$+Na), 555 (M) and 545 (M) which correspond to the ligand, MoO_2L(py), MoO_2L(γ-pic), MoO_2L(1–meth imz) and MoO_2L(THF) respectively (Fig. S3).

3.6. Electrochemistry

Cyclic Voltammograms of the complexes **1–4** were recorded at Pt electrode in dry degassed DMF containing 0.1 (M) TBAP as supporting electrolyte over a potential range 0.00 ± 1.50 V vs SCE. Results of cyclic voltammetric data are shown in the Table 1 and the representative diagram are shown in the Fig. 1 and Fig. S4. The complexes exhibited two irreversible one electron reduction processes in the potential range – 0.43 to – 0.62 V and – 1.06 to – 1.32 V due to Mo^{VI}/Mo^{V} and Mo^{V}/Mo^{IV} couples [46]. On scan reversal one irreversible two electron oxidative response was located at + 0.90 to + 0.99 V corresponding to Mo^{IV}/Mo^{VI} process [24]. It should be noted that the reduction of dioxo Mo(VI) complexes in aprotic solvents is generally irreversible.

3.7. Description of optimized geometries of the complexes and the nature of transition by DFT calculation

To interpret the electronic structures, full geometry optimizations of Mo(VI) complexes **1–4** were carried out in DFT/B3LYP method. The optimized structures of the four complexes **1–4** are given in Fig. 2, Fig. S5-S7 and important optimized geometrical parameters of the dioxomolybdenum(VI) complexes are listed in Table 2 and 3. The compositions along with their energies of some selected molecular orbitals of complexes are given in Table 4 and Table S1-S3. Contour plots of some selected frontier molecular orbitals of the complexes are shown in Fig. 3 and Fig. S8-S10. The higher energy occupied molecular orbitals (HOMO to HOMO-7) have ligand (L) contribution with 68–78% $p\pi$(S) contribution in

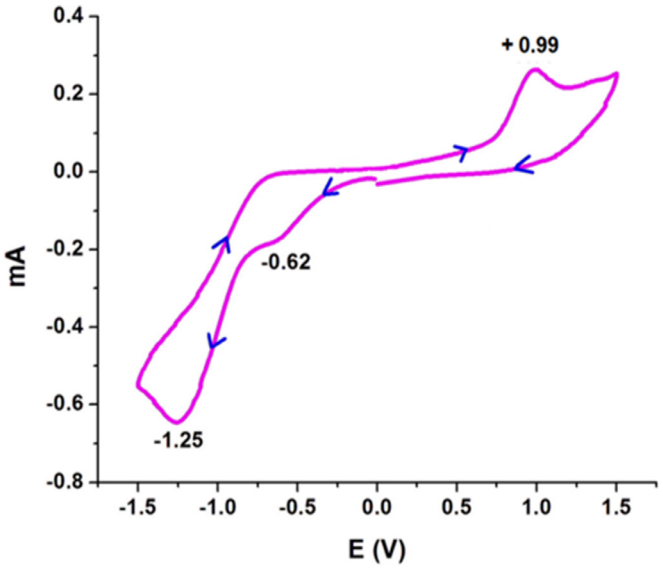

Fig. 1. Cyclic Voltammogram of MoO_2L(1-methyl imz) (**3**) in DMF at 298 K.

HOMO-2 and HOMO-3. The low energy unoccupied molecular orbitals (LUMO to LUMO+2) have mix $d\pi$(Mo) (30–58%) and π^*(L) (21–55%) character along with minor contributions of $p\pi$(O) (12–24%) orbital.

In the complex models for **1–4**, Mo(VI) center acquires a distorted octahedral geometry consisting of two *cis*-oxo atoms O(2), O(3); phenolate oxygen O(1), thioenolate sulfur S(1), azomethine nitrogen N(1) from the ligand and a donor atom X from the Lewis base [$X = N$(3) for complexes **1–3** and O(4) for complex **4**]. Three donor atoms from the ligand O(1), N(1), S(1) and oxo oxygen O(3) occupy the equatorial positions [47] where azomethine N(1) is trans to one oxo oxygen O(3) with N(1)-Mo(1)-O(3) bond angles 159.64°, 159.72°, 161.25°, 158.22° for the complexes **1–4** respectively. The ligand binds to the $[MoO_2]^{2+}$ core in tridentate binegative manner forming one five membered and one six membered stable metallocycles with bite angles N(1)-Mo(1)-S(1) and N(1)-Mo(1)-O(1) being 75.11°, 75.12°, 75.07°, 75.28° and 79.44°, 79.49°, 79.84°, 79.71° for the complexes **1–4** respectively [48].

Lewis bases like pyridine, γ-picoline, 1-methyl imidazole and THF coordinate to the vacant axial position *trans* to oxo oxygen O(2) with a bond angle O(2)-Mo(1)-N(3) being 171.82°, 171.41°, 169.18° for the complexes **1–3** and O(2)-Mo(1)-O(4) being 171.79° for complex **4** respectively [25]. The Mo-X [$X = N$(3) for complexes **1–3**, O(4) for complex **4**] bond lengths are slightly greater than the normal bond lengths due to strong *trans* influence of the terminal oxygen O(2). The Mo center is displaced from the median plane O(1),N(1),S(1),O(3) towards oxo oxygen O(2) by 0.371 Å, 0.366 Å, 0.336 Å, 0.387 Å respectively indicating small distortion in the octahedral geometry for the complexes. The Mo(1)-N(1), Mo(1)-O(1) and Mo(1)-S(1) bond lengths are very close in similar molybdenum(VI) complexes [49].

To get better insight into the electronic spectra of the complexes (**1–4**) vertical electronic excitations were calculated by TDDFT/CPCM method in methanol. The calculated excitation wavelength, their assignments and the corresponding oscillator strengths are summarized in Table 5 and Table S4. In the complexes very weak transitions at 420–433 nm correspond to HOMO-1 → LUMO transition having mixed ILCT and LMCT character ($(\pi(L)\rightarrow\pi^*(L)/d\pi(Mo)$). Again, the experimental absorption peak at 324–368 nm is found to mixed ILCT and LMCT character in the complexes. And the moderately intense transition at 212–234 nm corresponds to ILCT character.

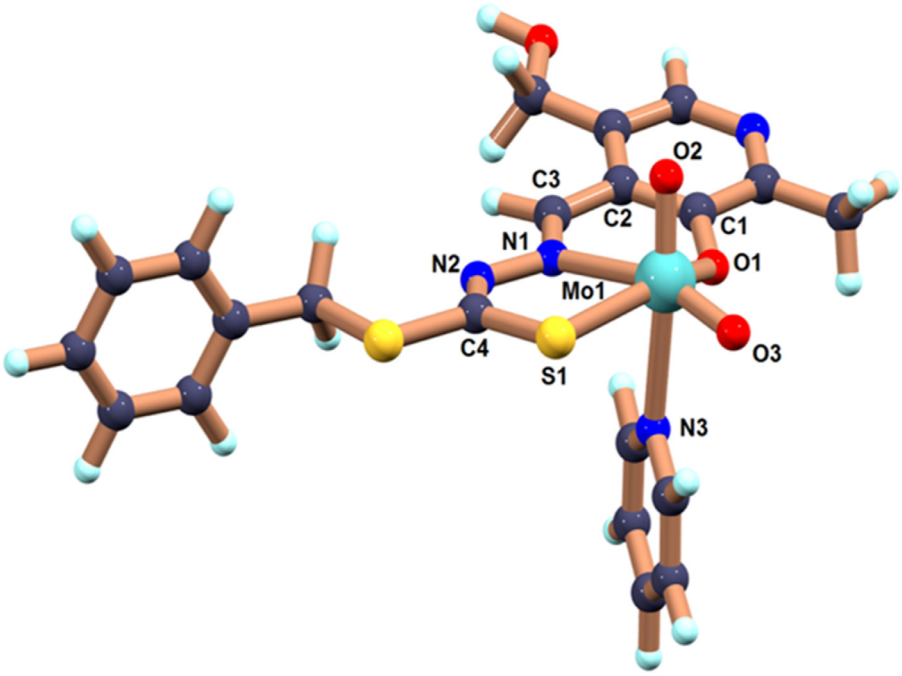

Fig. 2. Optimized structure of MoO_2L(py) (**1**).

Table 2
Bond distance (Å) parameters for the complexes **1–4**.

Bond distances (Å)	MoO_2L(py)(1)	MoO_2L(γ-pic)(2)	MoO_2L(1-methyl imz) (3)	MoO_2L(THF)(4)
Mo(1)-O(1)	1.979	1.978	1.987	1.972
Mo(1)-O(2)	1.712	1.709	1.711	1.704
Mo(1)-O(3)	1.721	1.718	1.715	1.717
Mo(1)-O(4)	–	–	–	2.537
Mo(1)-N(1)	2.339	2.337	2.349	2.323
Mo(1)-N(3)	2.567	2.556	2.511	–
Mo(1)-S(1)	2.472	2.474	2.476	2.467

Table 3
Bond angle (°) parameters for the complexes **1–4**.

Bond angles (°)	MoO_2L(py)(1)	MoO_2L(γ-pic)(2)	MoO_2L(1-methyl imz) (3)	MoO_2L(THF)(4)
S(1)-Mo(1)-O(3)	91.54	91.54	92.74	91.35
S(1)-Mo(1)-N(1)	75.11	75.12	75.07	75.28
N(1)-Mo(1)-O(1)	79.44	79.49	79.84	79.71
O(1)-Mo(1)-O(3)	106.55	106.71	106.33	105.41
O(2)-Mo(1)-S(1)	101.01	100.64	99.60	101.04
O(2)-Mo(1)-N(1)	91.25	91.08	90.02	93.15
O(2)-Mo(1)-O(1)	99.23	99.05	97.92	100.21
O(2)-Mo(1)-O(3)	106.58	106.71	106.26	106.42
S(1)-Mo(1)-X[a]	80.77	80.49	82.08	80.33
N(1)-Mo(1)-X[a]	81.46	80.91	80.04	79.32
O(1)-Mo(1)-X[a]	75.89	76.09	76.24	75.38
O(2)-Mo(1)-X[a]	171.82	171.41	169.18	171.79
O(3)-Mo(1)-X[a]	81.26	81.77	84.25	81.56
O(3)-Mo(1)-N(1)	159.64	159.72	161.25	158.22
O(1)-Mo(1)-S(1)	147.61	147.95	149.23	147.83

[a]$X = N(3)$ for complexes **1–3**, O(4) for MoO_2L(THF) (**4**).

3.8. Study of reactivity

A mixture of MoO_2L(py) (**1**) (0.55 g, 1.0 mmoL) and PPh_3 (0.39 g, 1.5 mmoL) are refluxed in dry degassed methanol medium for 1 h. The yellow solution readily changes to dark brown color with precipitation of corresponding $Mo^{IV}OL$ complexes. The reaction may be represented as:

$$Mo^{VI}O_2LB + PPh_3 \rightarrow Mo^{IV}OL + OPPh_3 + B$$

which may be considered as a two electron redox/oxygen atom transfer process.

MoOL: Anal. Calcd. for $C_{16}H_{15}N_3O_3S_2Mo$ (%): C, 42.01; H, 3.28; N, 9.19; Mo, 21.01. Found: C, 41.95; H, 3.10; N, 9.00; Mo, 20.87. Selected IR (KBr Pellet), cm^{-1}: $\nu_{(O-H)}$ 3401 (br), $\nu_{(C=N)}$ 1590 (m), $\nu_{(Mo=O)}$ 945 (s), $\nu_{(Mo-N)}$ 694 (m), $\nu_{(Mo-S)}$ 477(m), $\nu_{(Mo=O\bullet\bullet\bullet Mo)}$ 824 (m). UV–Vis (MeOH) [λ_{max}/nm (ε/dm^3 $mol^{-1}cm^{-1}$)]: 255 (8300), 331 (11,400), 455 (10,400). ^{1}H NMR (DMSO–d_6, δ/ppm): (-CH=*N*)

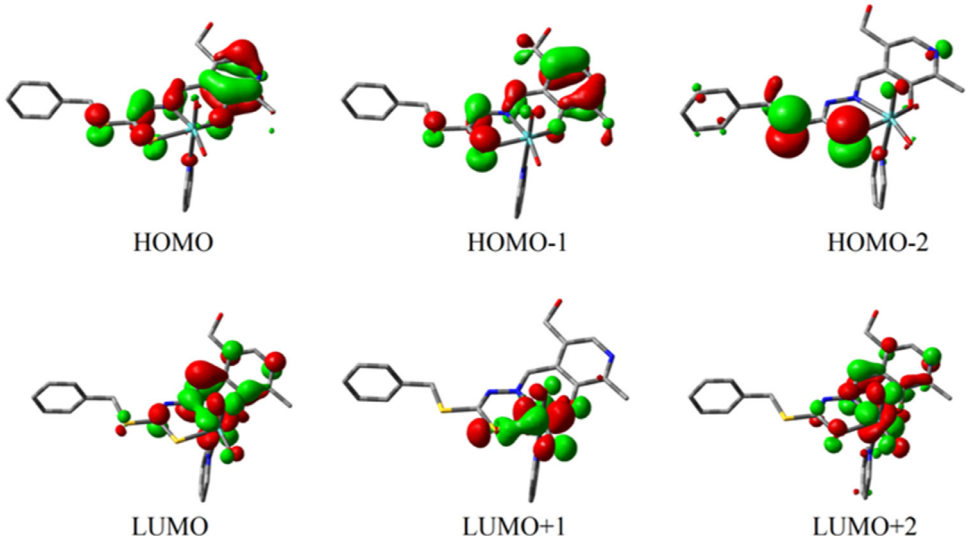

Fig. 3. Contour plots of selected molecular orbitals of $MoO_2L(py)$ (**1**).

Table 4
Energy and % of composition of $MoO_2L(py)$ (**1**).

MO	Energy (eV)	% Composition L	Mo	O	py
LUMO+5	−0.85	05	02	0	93
LUMO+4	−1.34	01	07	02	90
LUMO+3	−1.70	14	59	22	05
LUMO+2	−2.03	41	39	16	04
LUMO+1	−2.27	21	59	20	0
LUMO	−2.69	63	22	13	02
HOMO	−6.15	96	02	01	01
HOMO-1	−6.48	97	01	02	0
HOMO-2	−6.65	94	01	02	03
HOMO-3	−6.81	96	01	03	0
HOMO-4	−6.89	98	01	01	0
HOMO-5	−7.08	100	0	0	0
HOMO-6	−7.48	77	02	16	05
HOMO-7	−7.62	87	01	02	10
HOMO-8	−7.74	09	0	01	90
HOMO-9	−7.94	15	03	66	16
HOMO-10	−8.01	66	09	18	07

9.17 s (1H), (-S-CH_2-Ph) 4.46 s (2H), (Aromatic protons) 7.27–8.07 m (6H), (-CH_3) 2.38 s (3H), (-CH_2OH) 4.74 s (OH).

All other mononuclear complexes [$MoO_2L(\gamma$-pic)] (**2**), [MoO_2L(1-methyl imz)] (**3**) and [MoO_2L(THF)] (**4**) undergo oxo-transfer reactions under similar conditions as described above, which may be considered as a two electron redox/oxygen atom transfer process. The resulted $Mo^{IV}OL$ complexes are diamagnetic with d^2 (Mo^{IV}) electronic configuration. The complexes possess a strong IR stretching vibration at ~ 945cm^{-1} due to $\nu_{Mo=Ot}$ mode [50]. Another IR band of medium intensity arises around 824 cm^{-1} due to presence of polymeric Mo=*O*•••Mo linkages [51]. One representative diagram is shown in Fig. S11.

The electronic spectra of the Mo(IV) complexes have been checked in dry CH_3OH. The band around 300 nm in the parent complexes have been shifted to low energy 455 nm due to $L(p\pi) \rightarrow Mo(d\pi)$ LMCT transitions (Fig. S12).

Electrochemical studies further support the formation of Mo(IV) complexes. The complexes possess an irreversible two electron oxidative signal at around + 0.78 V for Mo^{IV}/Mo^{VI} couple, while on scan reversal two irreversible one electron responses are located at - 0.40 V and - 1.29 V corresponding to Mo^{VI}/Mo^{V} and Mo^{V}/Mo^{IV} processes respectively [50] (Fig. 4).

3.9. Protein interaction study

3.9.1. Absorption titration

Serum albumins (SA) are most abundant proteins in plasma and are involved in binding, transporting and delivering a variety of therapeutic drugs in the blood stream to their target organs [52].

A popular method to find out the type of quenching (static or dynamic) is through careful examination of the absorption spectra of BSA in presence of investigated compounds. For this absorp-

Table 5
Vertical electronic transitions of $MoO_2L(py)$ (**1**) calculated by TDDFT/CPCM method in methanol.

Compound	λ (nm)	E (eV)	Osc.Strength (f)	Key excitations	Character	$\lambda_{expt.}$ (nm)
$MoO_2L(py)$ (**1**)	475.9	2.61	0.0215	(93%)HOMO→LUMO	$\pi(L) \rightarrow \pi^*(L)/d\pi(Mo)$ ILCT/LMCT	
	405.8	3.05	0.0550	(83%)HOMO-1→LUMO	$\pi(L) \rightarrow \pi^*(L)/d\pi(Mo)$ ILCT/LMCT	420 (sh)
	369.7	3.35	0.1450	(67%)HOMO→LUMO+2	$\pi(L) \rightarrow \pi^*(L)/d\pi(Mo)$ ILCT/LMCT	368 (sh)
	330.7	3.75	0.0823	(37%)HOMO-7→LUMO (32%)HOMO-1→LUMO+2	$\pi(L) \rightarrow \pi^*(L)/d\pi(Mo)$ ILCT/LMCT	332
	316.1	3.92	0.1049	(67%)HOMO-8→LUMO	$\pi(L) \rightarrow \pi^*(L)/d\pi(Mo)$ ILCT/LMCT	
	222.9	5.56	0.0723	(53%)HOMO-2→LUMO+5	$\pi(L) \rightarrow \pi^*(L)$ ILCT	234

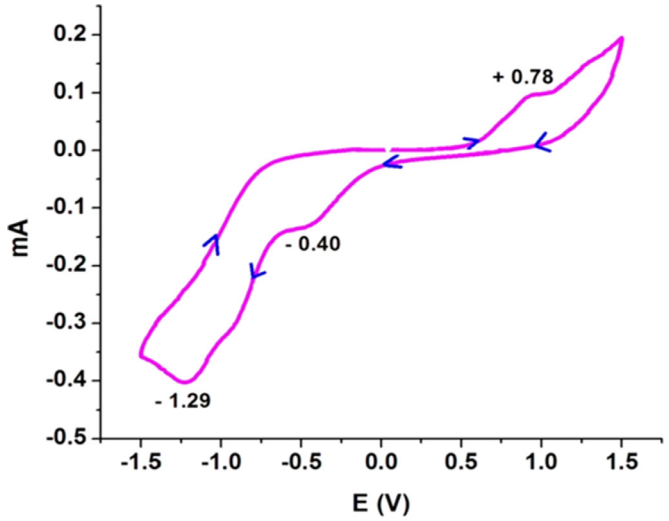

Fig. 4. Cyclic Voltammogram of $MoO^{IV}L$ in DMF at 298 K.

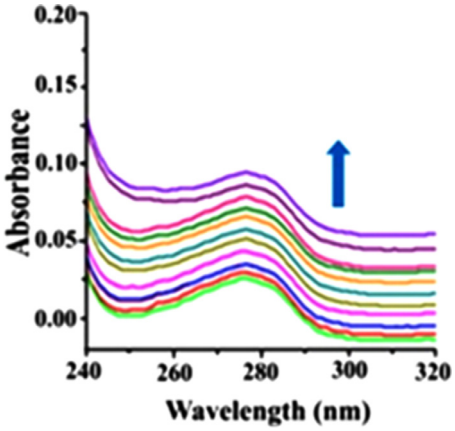

Fig. 5. Absorption spectra of 10^{-5} M BSA with incremental amounts of 10^{-4} M (0–20 μL) $MoO_2L(py)$ (**1**) at 298 K.

tion spectra of BSA were monitored in aqueous solution at pH = 7 (phosphate buffer) at room temperature. It was observed that initially BSA shows an absorption peak at 278 nm, the absorption intensity of BSA is found to enhance (hyperchromism) upon the gradual addition of the compounds (0–20 µL) along with a very slight blue shift of 1–3 nm (Fig. 5, Fig. S13).

3.9.2. Fluorescence quenching study

Fluorescence spectroscopy is the most important tool to investigate the interaction between the bioactive material with the biomolecules because it can provide interesting informations regarding modes of quenching, conformational and dynamic change in protein. BSA has three fluorophores namely tryptophan (Trp), tyrosine (Tyr) and phenyl alanine (Phe) of which tryptophan is responsible for the intrinsic fluorescence of BSA [53]. Change in the emission spectra of BSA is in response to protein conformational transitions, substrate binding or denaturation [54].

In our present study fluorescence emission spectra of BSA are recorded in absence and in presence of compounds (quenchers). In absence of quenchers BSA gives strong emission band at 356 nm upon excitation at 278 nm. The intensity of fluorescence spectra is found to decrease in a consistent manner with gradual increase in the quencher concentrations (0–20 µL) accompanied with a slight blue shift of 1–2 nm. The concentration dependent quenching of protein fluorescence by the compounds is given in Fig. 6, Fig. S14.

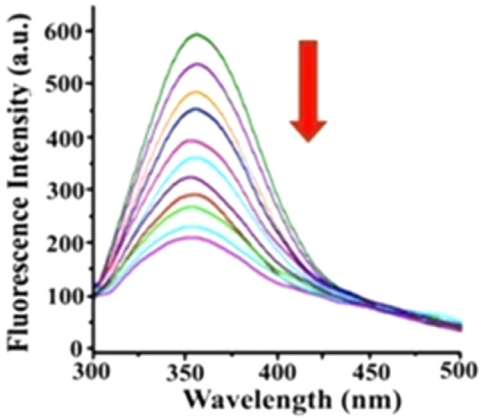

Fig. 6. Fluorescence quenching spectra of 10^{-5} M BSA with incremental amount of 10^{-4} M (0–20 µL) $MoO_2L(py)$ (**1**) at 298 K, (λ_{ex} = 278 nm).

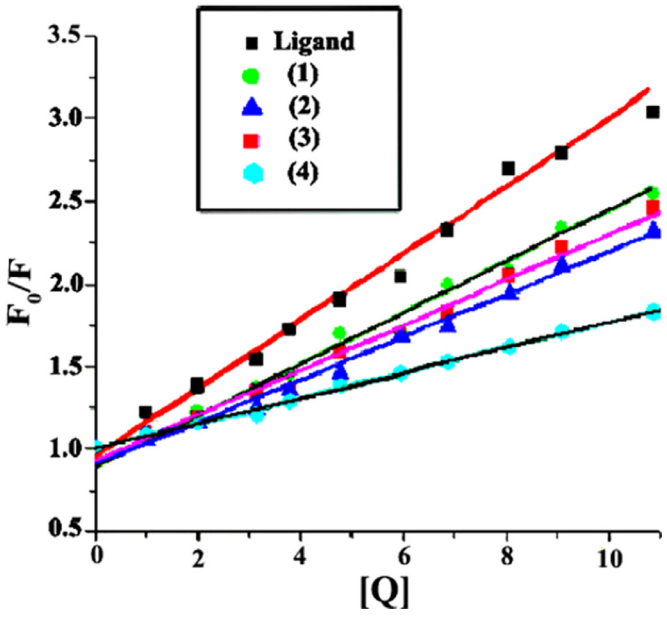

Fig. 7. Stern-Volmer plots of the ligand and the complexes (**1–4**) with BSA.

The observations suggest that there must be change in the fluorophoric environment of BSA protein due to interactions with the compounds [55]. A slight blue shift can be explained by the binding of the compound in the hydrophobic part of BSA.

In order to understand quantitatively the magnitudes of binding between BSA and the compounds fluorescence quenching data are analyzed with the help of Stern-Volmer equation [56]:

$$F_0/F = 1 + K_{SV}[Q] = 1 + k_q.\tau_0[Q]$$

where, F and F_0 are the fluorescence intensities, with and without quencher respectively, K_{SV} is the Stern-Volmer constant, [Q] is the concentration of the quencher, k_q is the bimolecular quenching rate constant and τ_0 is the average lifetime of the fluorophore BSA in absence of quencher. The plot of F_0/F vs [Q] (Fig. 7) is linear with a positive intercept nearly equal to one for both ligand and complexes. The quenching constant K_{SV} can be obtained from the slope of the graph and the values lie in the order of 10^6 indicating high quenching abilities. Bimolecular quenching rate constant (k_q) values for the ligand and the complexes are higher ($>10^{12}\ M^{-1}\ s^{-1}$) than diverse kinds of quenchers for biopolymer fluorescence ($2.0 \times 10^{10}\ M^{-1}\ s^{-1}$) and lie in the order of 10^{15} and 10^{14} respectively which confirms that the possible mode of quenching is static [57].

Table 6
Stern-Volmer constant ($\mathbf{K_{SV}}$), bimolecular quenching rate ($\mathbf{k_q}$), binding constant ($\mathbf{K_b}$) and number of biding sites (**n**) of the ligand (H_2L) and complexes (**1–4**).

Compounds	K_{SV} (M^{-1})	k_q ($M^{-1}\,s^{-1}$)	K_b (M^{-1})	n
Ligand (H_2L)	2.04×10^6	1.21×10^{15}	1.12×10^6	0.96
MoO_2L(py) (1)	1.56×10^6	5.04×10^{14}	5.13×10^6	1.09
MoO_2L(γ-pic) (2)	1.37×10^6	2.72×10^{14}	5.62×10^6	1.12
MoO_2L(1-methyl imz) (3)	1.29×10^6	4.03×10^{14}	6.92×10^6	1.13
MoO_2L(THF) (4)	0.76×10^6	1.39×10^{14}	1.07×10^6	1.03

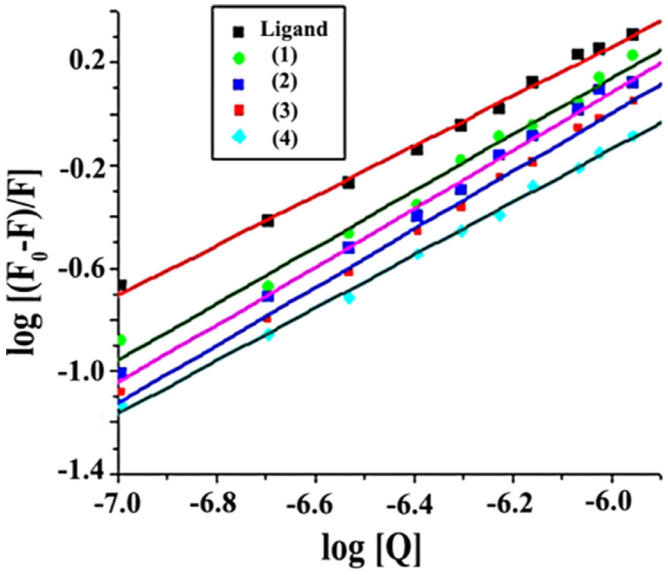

Fig. 8. Plot of log [(F_0-F)/F] vs log [Q] for the ligand and the complexes (**1–4**).

The binding constant K_b and the number of binding sites (n) can be calculated using the following equation [58]:

$$\log[(F_0 - F)/F] = \log K_b + n \log [Q]$$

From the plot of log [(F_0-F)/F] versus log [Q] (Fig. 8) the number of binding sites per albumin (n) is obtained from the slope and binding constant (K_b) is obtained from the intercept. K_{SV}, K_b and n values for the complexes are given in Table 6. Sufficiently high values of K_b indicate reversible binding and the release of compounds from BSA. From the above observations, it has been found that the binding constants lie in the order **3** > **2** > **1** > **H_2L** > **4**. Close examinations on the K_b values reveal that the complexes containing methyl substitution have higher binding abilities with BSA. Electron donating ability of methyl group increases electron density on ring nitrogen and enhances the extent of non-covalent interactions with the protein molecule. At the experimental temperature, number of binding sites is nearly equal to one for ligand and all the complexes implying there is only one binding site per BSA molecule.

3.9.3. Fluorescence resonance energy transfer (FRET)

Fluorescence Resonance Energy Transfer (FRET) is a non-radiative process that can be used to monitor the proximity and the relative orientation of the fluorophores [59]. The FRET process occurs when there is an appreciable overlap between the emission spectra of the donor and the absorption spectra of the acceptor. An essential criteria for energy transfer to take place is the distance between donor and the acceptor must be within the specified Förster distance of 2–8 nm.

This quenching of fluorescence is due to the energy transfer from the excited state of BSA to the ligand and complexes.

Fig. 9 and Fig. S15 shows that the emission spectra of tryptophan (Trp) residue of BSA and the absorption spectra of ligand and the complexes have appreciable overlap. The FRET efficiency can be calculated by using the following equation

$$E = R_0{}^6/\left(R_0{}^6 + r^6\right) = 1 - F/F_0$$

where F and F_0 are the fluorescence intensity of BSA after and before the addition of the ligand and complexes respectively, 'r' is the distance between the donor and the acceptor during the energy transfer process and R_0 is the critical distance when the efficiency is 50%. The value of R_0 can be calculated using the equation:

$$R_0 = 8.79 \times 10^{-25} k^2 n^{-4} \varphi J$$

Where k^2 is the orientation factor related to the geometry of the donor acceptor dipole and for the random orientation of the donor and acceptor a value of 2/3 is assumed for the value of k^2. 'n' stands for the refractive index of the medium and it is 1.34 for BSA solution in phosphate buffer (pH = 7.0). The fluorescence quantum yield for BSA is found to be 0.15. J is the overlap integral for the spectral overlap between the emission spectra of the donor (BSA) and the absorption spectra of the acceptor (compounds). J is defined as

$$J = \int F(\lambda)\varepsilon(\lambda)\lambda^4 d\lambda / \int F(\lambda) d\lambda$$

Where $F(\lambda)$ is the fluorescence intensity of the donor at wavelength λ and $\varepsilon(\lambda)$ is the molar extinction coefficient of the acceptor at wavelength λ. The calculated values of J, R_0, r and E are given in the Table S5.

From the calculated data it is observed that the donor acceptor distance is in the range of 2.49–3.82 nm which indicates that the energy transfer between BSA and the compounds occur with high probability.

3.9.4. Time resolved fluorescence measurement

Fluorescence life time measurement is one of the important techniques to investigate the nature of binding between the compounds with BSA protein. To investigate the excited state behavior and the microenvironment around the compounds, we have measured the fluorescence life time of the intrinsic fluorophore BSA with increasing concentrations of compounds (ligand and the complexes). The representative diagrams are shown in Fig. 10 and S16. Fluorescence decay curves are usually multiexponential in the case of compounds-protein binding process. The decay curves are fitted by biexponential function which generates two components of lifetime τ_1 and τ_2.

The decay profile has two components, τ_1 and τ_2. The contribution of τ_1 (α_1) is more than τ_2 (α_2) in case of free ligand and τ_2 in case of the complex (Table S6). The value of τ_1 in case of free ligand remains almost constant with increasing concentration of the compounds which reveals that the quenching is static in nature. However, very small decrease in τ_2 for ligand and τ_1 for complexes with higher concentration of the compounds may be due to FRET.

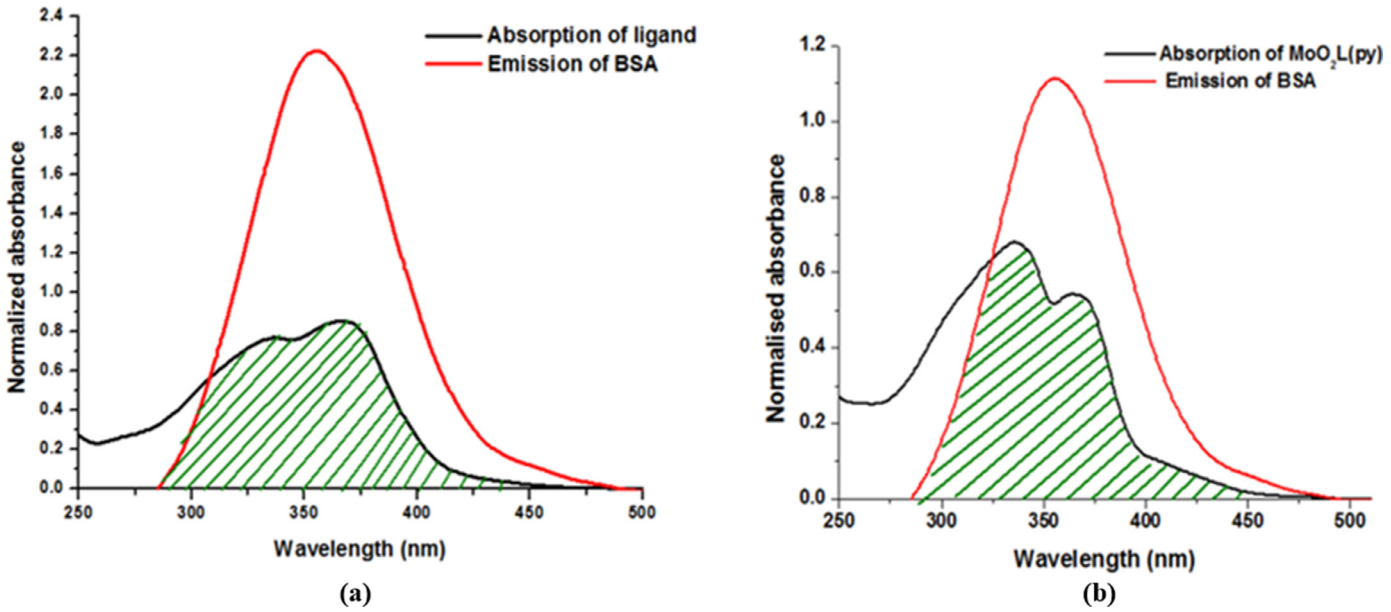

Fig. 9. Overlap of emission spectra of BSA and the absorption spectra of **(a)** Ligand and **(b)** $MoO_2L(py)$ (**1**).

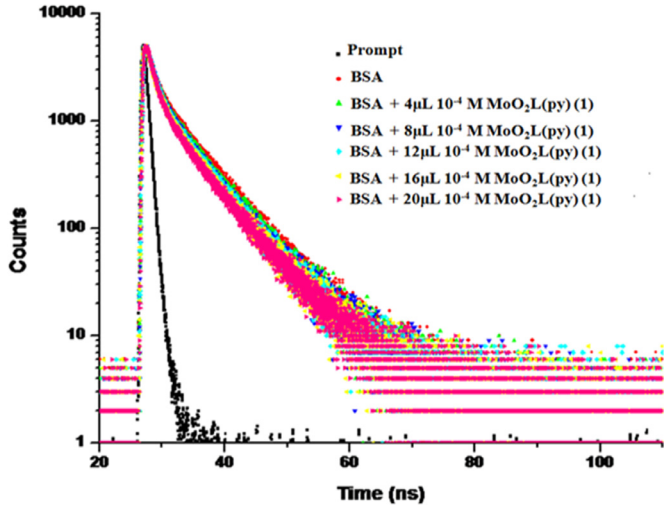

Fig. 10. Fluorescence decay curves of BSA with increasing concentrations of $MoO_2L(py)$ (**1**) (λ_{ext} = 291 nm).

3.9.5. Molecular docking studies

Molecular docking is a well established computational technique for prediction of the interactions between the molecules and macromolecules. Also, it is useful in determining the preferred binding site, binding character and optimized orientations of the molecule, which results in a new complex with overall minimum energy. The ligand and all the synthesized molybdenum complexes (**1**–**4**) were docked (Fig. 11, Fig. S17-S20). Crystal structure of BSA displays three homologous domains [I [(residues1–183), II (residues 184–376) and III (residues 377–583)] and each domains are distinguished with two sub-domains, A and B [60]. Sub-domains IIA or IIIA, popularly known as Sudlow's sites I and II respectively [61] are the most probable binding sites of the compounds with BSA. From docking analysis it has been observed that Ligand (H_2L), $MoO_2L(py)$ (**1**), $MoO_2L(\gamma$-pic) (**2**), MoO_2L(1-methyl imz) (**3**) and $MoO_2L(THF)$ (**4**) are preferably bound to Sudlow's site II (IIIA) over Sudlow's site I (IIA). Also, we have given a comparison of binding energies due to binding at Sudlow's site I & II to provide quantitative comparison of binding of each ligand in Table S7. All the compounds display better binding at to Sudlow's site II (IIIA) with higher binding energy. In addition, binding interactions, binding energies, ligand efficiency and inhibition constants for all the compounds with the amino acid residues of BSA are summarized in Table S8. The binding energies of the BSA-compound pairs follow the order BSA- MoO_2L(1-methyl imz) (**3**) > BSA- $MoO_2L(\gamma$-pic) (**2**) > BSA- $MoO_2L(py)$ (**1**) > BSA- Ligand (**H_2L**) > BSA- $MoO_2L(THF)$ (**4**) which is consistent with the fluorescence spectroscopic results. MoO_2L(1-methyl imz) (**3**) having highest binding energy (–17.20 kJ mol^{-1}) is surrounded by maximum number (13) of amino acid (both hydrophobic as well as polar) residues (TYR 496, VAL 497, PRO 498, LYS 499, ALA 500, PHE 501, HIS 534, LYS 535, PRO 536, LYS 537, ALA 538, LEU 582, ALA 583) and involved in hydrogen bonding with HIS-534 with bond length 2.4 Å. On the other hand, Ligand (H_2L), $MoO_2L(py)$ (**1**), $MoO_2L(\gamma$-pic) (**2**) and $MoO_2L(THF)$ (**4**) are surrounded by both hydrophobic as well as polar moieties namely (PRO 415, GLN 416, TYR 496, VAL 497, PRO 498, LYS 499, ALA 500), (GLN 416, VAL 468, THR 495, TYR 496, VAL 497, LYS 499), (LYS 504, THR 507, PHE 508, HIS 509, ASP 511, ILE 512, LEU 515, LYS 523), and (PRO 415, GLN 416, VAL 417, SER 418, VAL 468, TYR 496, VAL 497, PRO 498, LYS 499, ALA 500, LYS 533) respectively. Thus, we observed that except $MoO_2L(THF)$ (**4**), other ligands (H_2L), $MoO_2L(py)$ (**1**), $MoO_2L(\gamma$-pic) (**2**) and MoO_2L(1-methyl imz) (**3**) involve in hydrogen bonding with BSA with hydrogen bond length 2.0 Å, 3.2 Å, 2.3 Å and 2.4 Å respectively. This might be the possible reason behind minimum binding energy of $MoO_2L(THF)$ (**4**) in comparison to others. Besides, within 4 Å range surrounding the compounds, the number of hydrophobic moieties increased gradually, 6 for $MoO_2L(py)$ (**1**), 8 for $MoO_2L(\gamma$-pic) (**2**) and 13 for MoO_2L(1-methyl imz) (**3**). Binding energy also followed the same trend. Zhang et al., stated that increase of hydrophobic environment surrounding the ligand is a measure of increased stability [62]. All these compounds (H_2L, **1, 2**, and **3**) involve in hydrogen bonding, but hydrophobic interactions altered the extent of binding of the Mo complexes with BSA. In addition, polar residues like LYS 499/ LYS 535/ LYS 537 played a vital role to stabilize the ligand-BSA pairs. Thus, theoretical docking analysis well argued the observed spectroscopic results at molecular level and provides strong evidence in favor of fluores-

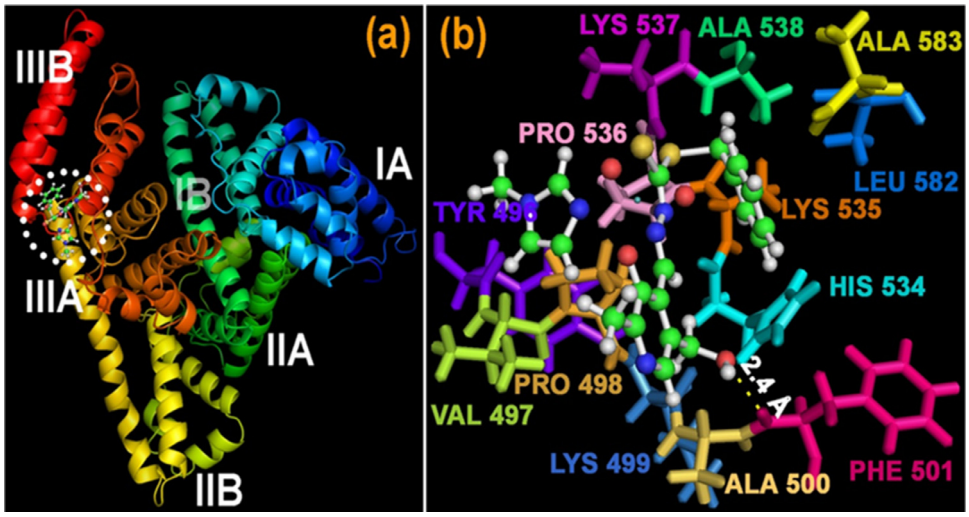

Fig. 11. (a) Molecular docked structure of MoO_2L(1-methyl imz) (**3**) with 3D structure of BSA (PDB ID: 3V03), docking pose is highlighted with white dotted circle; (b) Magnified view (within 4 Å around the MoO_2L(1-methyl imz) (**3**)**,** presented in ball and stick) of the binding site in the sub-domain of IIIA along with hydrogen bond distance.

cence quenching study observed as a combined effect of hydrogen bonding, hydrophobic forces and polar interactions.

4. Conclusion

Four mononuclear dioxomolybdenum(VI) complexes having general formula MoO_2LB with ONS donor ligand have been synthesized by varying Lewis bases. The complexes have been successfully characterized by several spectroscopic techniques like IR, UV–Vis, ^{1}H NMR, mass spectrometry. The electrochemical behavior of the complexes was examined by cyclic voltammetry. The molecular geometries of the complexes are established with the help of DFT calculations. The results of absorption and fluorescence titrations of the ligand and the complexes with protein BSA reveal that both of them bind with the protein in 1:1 ratio. Both the steady state and time resolved fluorescence results show that the mode of binding is static in nature. Fluorescence measurement indicates strong fluorescence energy transfer for BSA to the ligand and the complexes. The Förster distances of the ligand and the complexes have been calculated and they are in good agreement for the appreciable overlap. The results of molecular docking reveal that there is a hydrophobic and hydrogen bonding interactions between the compounds (ligand and the complexes) and BSA.

Supplementary information

Supplementary figures **S1, S2** and **S3** represent IR, electronic and mass spectra of the compounds respectively. **Fig. S4** shows the cyclic voltammograms of the complexes MoO_2L(py) (**1**), MoO_2L(γ-pic) (**2**) and MoO_2L(THF) (**4**). **Fig. S5-S7** contains optimized structures of the complexes **2**–**4. Fig. S8-S10** contains the contour plots of the selected molecular orbitals of the complexes **2**–**4. Fig. S11** and **S12** represent IR and electronic spectra of one representative Mo(IV) complex. Absorption spectra and quenching spectra of 10^{-5} M BSA with incremental amount of the ligand and complexes **2**–**4** are given in **Fig. S13** and **S14** respectively. FRET diagrams and fluorescence decay curves of the ligand and the complexes are given in **Fig. S15** and **S16** respectively. Molecular docked structures of the ligand and complexes **1, 2, 4** are shown in **Fig. S17-S20. Table S1-S3** represent the energy and % of composition of the complexes **2, 3, 4**. Vertical electronic transitions of complexes **2, 3, 4** are given in **Table S4**. FRET parameters and the variation of lifetime of BSA during titrations are shown in **Table S5-S6**. The comparison of binding energy of H_2L and its Mo complexes due to binding at Sudlow's Site I (IIA) and II (IIIA) is given in **Table S7**. Docking results of BSA and Ligand (H_2L) along with its MoO_2LB complexes (**1**–**4**) are listed in **Table S8**.

Declaration of Competing Interest

The authors declare that they have no known competing financial interests or personal relationships that could have appeared to influence the work reported in this paper.

Acknowledgment

There is no funding body to report.

Supplementary materials

Supplementary material associated with this article can be found, in the online version, at doi:10.1016/j.molstruc.2021.130192.

References

[1] R.C. Bray, The inorganic biochemistry of molybdoenzymes, Quart. Rev. Biophys. 21 (1988) 299–329, doi:10.1017/S0033583500004479.
[2] R.H. Holm, J.M. Berg, Toward functional models of metalloenzyme active sites: analogue reaction systems of the molybdenum oxo transferases, Acc. Chem. Res. 19 (1986) 363–370, doi:10.1021/ar00131a006.
[3] W.H. Orme-Johnson, Molecular basis of biological nitrogen fixation, Ann. Rev. Biophys. Biophys. Chem. 14 (1985) 419–459, doi:10.1146/annurev.bb.14.060185.002223.
[4] C.J. Doonan, D.J. Nielsen, P.D. Smith, J.M. White, G.N. George, C.G. Young, Models for the molybdenum hydroxylases: synthesis, characterization and reactivity of *cis*-oxosulfido-Mo(VI) complexes, J. Am. Chem. Soc. 128 (2006) 305–316, doi:10.1021/ja056109u.
[5] M.R. Maurya, S. Dhaka, F. Avecilla, Synthesis, characterization, reactivity and catalytic activity of dioxidomolybdenum(VI) complexes derived from tribasic ONS donor ligands, Polyhedron 81 (2014) 154–167, doi:10.1016/j.poly.2014.05.068.
[6] R.R. Schrock, Recent advances in olefin metathesis by molybdenum and tungsten imido alkylidene complexes, J. Mol. Catal. A: Chem. 213 (2004) 21–30, doi:10.1016/j.molcata.2003.10.060.
[7] R.K. Grasselli, Advances and future trends in selective oxidation and ammoxidation catalysis, Catal. Today. 49 (1999) 141–153, doi:10.1016/S0920-5861(98)00418-0.
[8] M. Chakraborty, S. Roychowdhury, N.R. Pramanik, T.K. Raychaudhuri, T.K. Mondal, S. Kundu, M.G.B. Drew, S. Ghosh, S.S. Mandal, Synthesis, characterization, crystal structure and density functional theory (DFT) calculations of dioxomolybdenum (VI) complexes of an ONS donor ligand derived from benzoylacetone and S-benzyl dithiocarbazate, Polyhedron 50 (2013) 602–611, doi:10.1016/j.poly.2012.12.006.

[9] J. Awapara, R.P. Sandman, C. Hanly, Activation of DOPA decarboxylase by pyridoxal phosphate, Biochem. Biophys. 98 (1962) 520–525, doi:10.1016/0003-9861(62)90220-5.

[10] T. Matsuo, Y. Sadzuka, In vitro anticancer activities of B6 vitamers: a mini-review, Anticancer Res. 39 (2019) 3429–3432, doi:10.21873/anticancers.13488.

[11] M.R. Maurya, S. Khurana, A. Azam, W. Zhang, D. Rehder, Shailendra, Synthesis, characterisation and antiamoebic studies of dioxovanadium(V) complexes containing ONS donor ligands derived from S-benzyldithiocarbazate, Eur. J. Inorg. Chem. (2003) 1966–1973, doi:10.1002/ejic.200200642.

[12] J.H.K.A. Acquaye, M.F. Richardson, Palladium and platinum complexes with vitamin B6 compounds, Inorg. Chim. Acta. 201 (1992) 101–107, doi:10.1016/S0020-1693(00)85009-4.

[13] S. Naskar, S. Naskar, H.M. Figgie, W.S. Sheldrick, S.K. Chattopadhyay, Synthesis, crystal structures and spectroscopic properties of two Zn(II) Schiff's base complexes of pyridoxal, Polyhedron 29 (2010) 493–499, doi:10.1016/j.poly.2009.06.040.

[14] K. Hirayama, S. Akashi, M. Furuya, K. Fukuhara, Rapid confirmation and revision of the primary structure of bovine serum albumin by ESIMS and FRIT-FAB LC/MS, Biochem. Biophys. Res. Commun. 173 (1990) 639–646, doi:10.1016/S0006-291X(05)80083-X.

[15] M.B. Pereira, C.R. Kopp, L.A. Fontana, G.M. de Oliveira, D.F. Back, P.C. Piquini, M.A. Villetti, Synthesis, X-ray structural features, DFT calculations and fluorescence studies of a new pyridoxal-benzimidazole ligand and its respective molybdenum complex, New J. Chem. 38 (2014) 3092–3101, doi:10.1039/c4nj00259h.

[16] J. Pisk, B. Prugovecki, D.M. Calogovic, T. Jednacak, P. Novak, D. Agustin, V. Vrdoljak, Pyridoxal hydrazonato molybdenum(VI) complexes: assembly, structure and epoxidation (pre)catalyst testing under solvent-free conditions, RSC Adv. 4 (2014) 39000–39010, doi:10.1039/c4ra08179j.

[17] V. Vrdoljak, J. Pisk, B. Prugovecki, D.M. Calogovic, Novel dioxomolybdenum(VI) and oxomolybdenum(V) complexes with pyridoxal thiosemicarbazone ligands: synthesis and structural characterization, Inorg. Chim. Acta. 362 (2009) 4059–4064, doi:10.1016/j.ica.2009.05.057.

[18] M. Das, S.E. Livingstone, Metal chelates of dithiocarbazic acid and its derivatives. IX. Metal chelates of ten new Schiff bases derived from S-methyldithiocarbazate, Inorg. Chim. Acta. 19 (1976) 5–10, doi:10.1016/S0020-1693(00)91065-X.

[19] G.J. Chen, J.W. McDonald, W.E. Newton, Synthesis of Mo(IV) and Mo(V) complexes using oxo abstraction by phosphines. mechanistic implications, Inorg. Chem. 15 (1976) 2612–2615, doi:10.1021/ic50165a008.

[20] K.A. Crouse, K.-.B. Chew, M.T.H. Tarafder, A. Kasbollah, A.M. Ali, B.M. Yamin, H.-.K. Fun, Synthesis, characterization and bio-activity of S-2-picolyldithiocarbazate (S2PDTC), some of its Schiff bases and their Ni(II) complexes and X-ray structure of S-2-picolyl-β-N-(2-acetylpyrrole)dithiocarbazate, Polyhedron 23 (2004) 161–168, doi:10.1016/j.poly.2003.09.025.

[21] S.A. Elsayed, A.M. Noufal, A.M. El-Hendawy, Synthesis, structural characterization and antioxidant activity of some vanadium(IV), Mo(VI)/(IV) and Ru(II) complexes of pyridoxal Schiff base derivatives, J. Mol. Struc. 1144 (2017) 120–128, doi:10.1016/j.molstruc.2017.05.020.

[22] A.D. Becke, Density-functional thermochemistry. III. The role of exact exchange, J. Chem. Phys. 98 (1993) 5648–5652, doi:10.1063/1.464913.

[23] C. Lee, W. Yang, R.G. Parr, Development of the Colle-Salvetti correlation- energy formula into a functional of the electron density, Phys. Rev. B. 37 (1988) 785–789, doi:10.1103/PhysRevB.37.785.

[24] N.R. Pramanik, M. Chakraborty, D. Biswal, S.S. Mandal, S. Ghosh, S. Chakrabarti, W.S. Sheldrick, M.G.B. Drew, T.K. Mondal, D. Sarkar, Binuclear dioxomolybdenum(VI) complexes of some tridentate ONS donor ligand containing $[MoO_2]^{2+}$ as the acceptor center: synthesis, crystal structure, supremolecular architectures via hydrogen bonds, π-π stacking and DFT calculations, Polyhedron 85 (2015) 196–207, doi:10.1016/j.poly.2014.08.010.

[25] D. Biswal, N.R. Pramanik, S. Chakrabarti, N. Chakraborty, K. Acharya, S.S. Mandal, S. Ghosh, M.G.B. Drew, T.K. Mondal, S. Biswas, Lewis base controlled supramolecular architectures *via* non-covalent interactions of dioxomolybdenum(VI) complexes with an ONS donor ligand: DFT calculations and biological study, New. J. Chem. 39 (2015) 2778–2794, doi:10.1039/c4nj02225d.

[26] H. Tanaka, A. Sasada, T. Kouno, M. Yuki, Y. Miyake, H. Nakanishi, Y. Nishibayashi, K. Yoshizawa, Molybdenum-catalyzed transformation of molecular dinitrogen into silylamine: experimental and DFT study on the remarkable role of ferrocenyldiphosphine ligands, J. Am. Chem. Soc. 133 (2011) 3498–3506, doi:10.1021/ja109181n.

[27] D. Andrae, U. Haeussermann, M. Dolg, H. Stoll, H. Preuss, Energy adjusted ab initio pseudopotentials of the second and third row transition elements, Theor. Chim. Acta. 77 (1990) 123–141, doi:10.1007/BF01114537.

[28] P. Fuentealba, H. Preuss, H. Stoll, L.V. Szentpaly, A proper account of core-polarization with pseudo potentials: single valance-electron alkali compounds, Chem. Phys. Lett. 89 (1982) 418–422, doi:10.1016/0009-2614(82)80012-2.

[29] R. Bauernschmitt, R. Ahlrichs, Treatment and electronic excitations within the adiabatic approximation of time dependent density functional theory, Chem. Phys. Lett. 256 (1996) 454–464, doi:10.1016/0009-2614(96)00440-X.

[30] R.E. Stratmann, G.E. Scuseria, M.J. Frisch, An efficient implementation of time-dependent density-functional theory for the calculation of excitation energies of large molecules, J. Chem. Phys. 109 (1998) 8218–8224, doi:10.1063/1.477483.

[31] M.E. Casida, C. Jamorski, K.C. Casida, D.R. Salahub, Molecular excitation energies to high-lying bound states from time-dependent density-functional response theory: characterization and correction of the time-dependent local density approximation ionization threshold, J. Chem. Phys. 108 (1998) 4439–4449, doi:10.1063/1.475855.

[32] V. Barone, M. Cossi, Quantum calculation of molecular energies and energy gradients in solution by a conductor solvent model, J. Phys. Chem. A. 102 (1998) 1995–2001, doi:10.1021/jp9716997.

[33] M. Cossi, V. Barone, Time-dependent density functional theory for molecules in liquid solutions, J. Chem. Phys. 115 (2001) 4708–4717, doi:10.1063/1.1394921.

[34] M. Cossi, N. Rega, G. Scalmani, V. Barone, Energies, structures and electronic properties of molecules in solution with the C-PCM solvation model, J. Comput. Chem. 24 (2003) 669–681, doi:10.1002/jcc.10189.

[35] Gaussian 09, Revision D.01, M.J. Frisch, G.W. Trucks, H.B. Schlegel, G.E. Scuseria, M.A. Robb, J.R. Cheeseman, G. Scalmani, V. Barone, B. Mennucci, G.A. Petersson, H. Nakatsuji, M. Caricato, X. Li, H.P. Hratchian, A.F. Izmaylov, J. Bloino, G. Zheng, J.L. Sonnenberg, M. Hada, M. Ehara, K. Toyota, R. Fukuda, J. Hasegawa, M. Ishida, T. Nakajima, Y. Honda, O. Kitao, H. Nakai, T. Vreven, J.A. Montgomery, Jr., J.E. Peralta, F. Ogliaro, M. Bearpark, J.J. Heyd, E. Brothers, K.N. Kudin, V.N. Staroverov, R. Kobayashi, J. Normand, K. Raghavachari, A. Rendell, J.C. Burant, S.S. Iyengar, J. Tomasi, M. Cossi, N. Rega, J.M. Millam, M. Klene, J.E. Knox, J.B. Cross, V. Bakken, C. Adamo, J. Jaramillo, R. Gomperts, R.E. Stratmann, O. Yazyev, A.J. Austin, R. Cammi, C. Pomelli, J.W. Ochterski, R.L. Martin, K. Morokuma, V.G. Zakrzewski, G.A. Voth, P. Salvador, J.J. Dannenberg, S. Dapprich, A.D. Daniels, Ö. Farkas, J.B. Foresman, J.V. Ortiz, J. Cioslowski, and D.J. Fox, Gaussian, Inc., Wallingford CT (2009).

[36] N.M. O'Boyle, A.L. Tenderholt, K.M. Langner, Software news and updates cclib: a library for package-independent computational chemistry algorithms, J. Comput. Chem. 29 (2008) 839–845, doi:10.1002/jcc.20823.

[37] G.M. Morris, D.S. Goodsell, R.S. Halliday, R. Huey, W.E. Hart, R.K. Belew, A.J. Olson, Automated docking using a lamarckian genetic algorithm and an empirical binding free energy function, J. Comput. Chem. 19 (1998) 1639–1662 https://doi.org/10.1002/(SICI)1096-987X(19981115)19:14>1639::AID-JCC10>3.0.CO;2-B.

[38] , The PyMOL Molecular Graphics System, Version 1.3, Schrodinger, LLC, Mannheim, Germany, 2010.

[39] Y. Yanai, D. Tew, N.C. Handy, A new hybrid exchange-correlation functional using the coulomb-attenuating method (CAM-B3LYP), Chem. Phys. Lett. 393 (2004) 51–57, doi:10.1016/j.cplett.2004.06.011.

[40] K.A. Majorek, P.J. Porebski, A. Dayal, M.D. Zimmerman, K. Jablonska, A.J. Stewart, M. Chruszcz, W. Minor, Structural and immunologic characterization of bovine, horse, and rabbit serum albumins, Mol. Immunol. 52 (2012) 174–182, doi:10.1016/j.molimm.2012.05.011.

[41] E.I. Stiefel, Coordination and bioinorganic chemistry of molybdenum, Prog. Inorg. Chem. 22 (1977) 1–223.

[42] N.R. Pramanik, S. Ghosh, T.K. Raychaudhuri, S. Chaudhuri, M.G.B. Drew, S.S. Mandal, Chemical, electrochemical and structural studies of some *cis*-dioxomolybdenum(VI) complexes of two tridentate ONS chelating ligands, J. Coord. Chem. 60 (2007) 2177–2190, doi:10.1080/00958970701258192.

[43] S.K. Dutta, D.B. McConville, W.J. Youngs, M. Chaudhury, Reactivity of Mo-O_t terminal bonds toward substrates having simultaneous proton- and electron-donor properties: a rudimentary functional model for oxotransferase molybdenum enzymes, Inorg. Chem. 36 (1997) 2517–2522, doi:10.1021/ic960670z.

[44] S. Purohit, A.P. Koley, L.S. Prasad, P.T. Manoharan, S. Ghosh, Chemistry of molybdenum with hard-soft donor ligands. 2.[1] Molybdenum(VI), -(V), and -(IV) oxo complexes with tridentate Schiff base ligands, Inorg. Chem. 28 (1989) 3735–3742, doi:10.1021/ic00318a024.

[45] N.R. Pramanik, S. Ghosh, T.K. Raychaudhuri, S. Ray, R.J. Butcher, S.S. Mandal, Synthesis, characterization and crystal structure of oxomolybdenum (VI) and (IV) complexes of some tridentate ONS donor ligands, Polyhedron 23 (2004) 1595–1603, doi:10.1016/j.poly.2004.03.010.

[46] R. Dinda, P. Sengupta, S. Ghosh, W.S. Sheldric, Synthesis, structure and reactivity of a new mononuclear molybdenum(VI) complex resembling the active center of molybdenum oxotransferases, Eur. J. Inorg. Chem. (2003) 363–369, doi:10.1002/ejic.200390049.

[47] R. Hahn, U. Kusthardt, W. Scherer, A spectroscopic model for the high pH form of sulfite oxidase, Inorg. Chim. Acta 210 (1993) 177–182, doi:10.1016/S0020-1693(00)83325-3.

[48] S.Roy Saswati, S.P. Dash, R. Acharyya, W. Kaminsky, V. Ugone, E. Garribba, C. Harris, J.M. Lowe, R. Dinda, Chemistry of oxidomolybdenum(IV) and -(VI) complexes with ONS donor ligands: synthesis, computational evaluation and oxo-transfer reactions, Polyhedron 141 (2018) 322–336, doi:10.1016/j.poly.2017.12.023.

[49] E.B. Seena, M.R. Prathapachandra Kurup, Synthesis of mono- and binuclear dioxomolybdenum(VI) complexes derived from N(4)-substituted thiosemicarbazones: x-ray crystal structures of $[(MoO_2L^1)_2]$, $[MoO_2L^1py]$ and $[MoO_2L^2py]$, Polyhedron 26 (2007) 3595–3601, doi:10.1016/j.poly.2007.03.046.

[50] N.R. Pramanik, S. Ghosh, T.K. Raychaudhuri, S.S. Mandal, Synthesis, chemical and electrochemical studies of oxomolybdenum(IV) complexes with two tridentate ONS donor ligands, J. Coord. Chem. 62 (2009) 3845–3852, doi:10.1080/00958970903176887.

[51] I.W. Boyed, J.T. Spence, Molybdenum(IV)-oxo complexes with oxygen, nitrogen, and sulfur ligands. syntheses and electrochemical studies, Inorg. Chem. 21 (1982) 1602–1606, doi:10.1021/ic00134a066.

[52] X.M. He, D.C. Carter, Atomic structure and chemistry of human serum albumin, Nature 358 (1992) 209–215, doi:10.1038/358209a0.

[53] Sułkowska, Interaction of drugs with bovine and human serum albumin, J. Mol. Struct. 614 (2002) 227–232, doi:10.1016/S0022-2860(02)00256-9.

[54] S.G. Kalaiarasi, P. Kalaivani, F. Dallemer, R. Prabhakaran, CT-DNA/BSA protein

binding and antioxidant studies of new binuclear Pd(II) complexes and their structural characterization, Inorg. Chim. Acta. 449 (2016) 107–118, doi:10.1016/j.ica.2016.05.018.
[55] P. Sathyadevi, P. Krishnamoorthy, R.R. Butorac, A.H. Cowley, N.S.P. Bhuvanesh, N. Dharmaraj, Effect of substitution and planarity of the ligand on DNA/BSA interaction, free radical scavenging and cytotoxicity of diamagnetic Ni(II) complexes: a systematic investigation, Dalton Trans. 40 (2011) 9690–9702, doi:10.1039/c1dt10767d.
[56] G. Cohen, H. Eisenberg, Viscosity and sedimentation study of sonicated DNA-proflavine complexes, Biopolymers 8 (1969) 45–55, doi:10.1002/bip.1969.360080105.
[57] H.Y. Liu, Z.H. Xu, X.H. Liu, P.X. Xi, Z.Z. Zeng, Analysis of binding interaction between bovine serum albumin and the cobalt(II) complex with salicylaldehyde-2-phenylquinoline-4-carbonylhydrazone, Chem. Pharm. Bull. 57 (2009) 1237–1242, doi:10.1248/cpb.57.1237.
[58] P. Krishnamoorthy, P. Sathyadevi, A.H. Cowley, R.R. Butorac, N. Dharmaraj, Evaluation of DNA binding, DNA cleavage, protein binding and in vitro cytotoxic activities of bivalent transition metal hydrazone complexes, Eur. J. Med. Chem. 46 (2011) 3376–3387, doi:10.1016/j.ejmech.2011.05.001.
[59] P.B. Kandagal, S. Ashoka, J. Seetharamappa, S.M.T. Shaikh, Y. Jadegoud, O.B. Ijare, Study of the interaction of an anticancer drug with human and bovine serum albumin: spectroscopic approach, J. Pharm. Biomed. Anal. 41 (2006) 393–399, doi:10.1016/j.jpba.2005.11.037.
[60] D.C. Carter, J.X. Ho, Structure of serum albumin, Adv. Protein Chem. 45 (1994) 153–203, doi:10.1016/S0065-3233(08)60640-3.
[61] M. Banerjee, U. Pal, A. Subudhhi, A. Chakrabarti, S. Basu, Interaction of merocyanine 540 with serum albumins: photophysical and binding studies, J. Photochem. Photobiol. B: Biol. 108 (2012) 23–33, doi:10.1016/j.jphotobiol.2011.12.005.
[62] Y. Zhang, Y. Li, L. Dong, J. Li, W. He, X. Chen, Z. Hu, Investigation of the interaction between naringin and human serum albumin, J. Mol. Struct. 875 (2008) 1–8, doi:10.1016/j.molstruc.2007.03.063.